J. Fluid Mech. (1994), *vol.* 280, *pp.* 287–302

Dissolving driven by vigorous compositional convection

By ROSS C. KERR

Research School of Earth Sciences, The Australian National University, Canberra, ACT 0200, Australia

(Received 11 March 1993 and in revised form 17 June 1994)

The one-dimensional dissolution that occurs when a binary melt is placed above or below a solid of a different composition is examined both theoretically and experimentally. In the case considered, the dissolution is driven by vigorous compositional convection that results from a Rayleigh–Bénard instability of the compositional boundary layer in the vicinity of the dissolving solid. A scaling analysis is used to derive theoretical expressions for both the dissolving velocity and the interfacial fluid concentration. Laboratory experiments are also described in which ice is dissolved when it is overlain or underlain by aqueous solutions. The measured dissolving velocities are consistent with the theoretical expressions, and yield estimates of the critical Rayleigh number for boundary-layer instability. The results of this study are then applied to predict the rate at which dissolution will occur when undersaturated mixed magmas are generated during the periodic replenishment of large basaltic magma chambers in the Earth's crust.

1. Introduction

Both the melting and the dissolving of solids in fluids are fundamental physical phenomena which are encountered daily; for example, whenever ice is melted in water or sugar dissolved in coffee. Melting occurs when the temperature of the fluid is significantly greater than the melting temperature of the solid, and is controlled by thermal diffusion (cf. Woods 1992; Kerr 1994; and the Appendix). In contrast, dissolving occurs at relatively lower fluid temperatures, and is due to chemical disequilibrium between the solid and fluid. It is controlled by compositional diffusion and will continue for as long as the fluid remains above its freezing temperature.

In the special case where both the thermal and compositional fields in the fluid are gravitationally stable, fluid mechanics does not play a role, and the rate at which either melting or dissolving occurs can be determined analytically (Woods 1992). Often however, either or both of the thermal and compositional fields will be unstable and convection will result. Convection invariably enhances the rate of melting or dissolving by assisting the transfer of heat and composition to the solid. Recent studies have quantified this rate in the one-dimensional cases of melting driven by forced turbulent flow (Huppert 1989), free thermal convection (Huppert & Sparks 1988*a*, *b*) and free compositional convection (Kerr 1994). In the latter case, compositional convection arises when a hot fluid melts an underlying solid, and the density of the melted solid is less than that of the fluid, or when the hot fluid melts an overlying solid whose melt density is greater than that of the fluid.

The present paper is a natural continuation of the above studies, and quantifies the rate of dissolution of a horizontal boundary in the presence of vigorous compositional

convection. I begin in §2 by using a scaling analysis to derive theoretical expressions for the temperature, concentration and velocity of the interface. These expressions are then compared in §3 with the results of a series of experiments in which either an ice floor or roof is dissolved in contact with aqueous solutions. The results are applied to replenished magma chambers in §4, and then summarized in §5.

2. Scaling theory

2.1. *Dissolving a floor*

Consider the dissolving of a solid of composition C_s, melting temperature T_m and far-field temperature T_s, overlain by a fluid with a composition C_f and temperature T_f. If the volume of fluid is large, the far-field conditions will not change, and it is expected that the solid dissolves at a constant velocity V. The resulting thermal and compositional profiles are shown in figure 1 and illustrated on a typical phase diagram in figure 2. At the interface between the solid and the fluid, the temperature T_i and composition C_i are constrained thermodynamically to lie on the liquidus curve

$$T_i = T_L(C_i), \tag{1}$$

which gives the freezing temperature of the fluid as a function of concentration. Within the solid, the temperature is given by

$$T(z) = T_s + (T_i - T_s)\,\mathrm{e}^{-Vz/\kappa_s} \tag{2}$$

(Carslaw & Jaeger 1986), where κ_s is the thermal diffusivity of the solid.

There are composition and thermal boundary layers immediately adjacent to the interface. If the respective fluxes to the interface through these layers are F_C and F_T, the effective layer thicknesses can be defined by

$$F_C = \frac{D(C_f - C_i)}{h_C} \quad \text{and} \quad F_T = \frac{k_f(T_f - T_i)}{h_T}, \tag{3a, b}$$

where D and k_f are the compositional diffusivity and thermal conductivity of the fluid. If the volume change associated with the phase change is neglected (cf. Woods 1992; Chiareli, Huppert & Worster 1994), the boundary-layer fluxes are also linked to the dissolving rate V by the interfacial conditions

$$F_C = V(C_i - C_s) \quad \text{and} \quad F_T = V(\rho_s L_s + \rho_s c_s(T_i - T_s)), \tag{4a, b}$$

where ρ_s, L_s and c_s are the density, latent heat and specific heat of the solid.

The aim is to use scaling theory to determine V in the case where dissolving of the solid leads to vigorous compositional convection, a situation which will occur if the density ρ_i of the fluid at the interface is sufficiently less than the density ρ_f of the far-field fluid. I assume that the interface between the solid and the fluid is flat, and that the unstable compositional buoyancy released at the interface dominates the stabilizing thermal buoyancy, i.e. that the ratio $\mathscr{R}$ of these buoyancies satisfies the condition

$$\mathscr{R} \equiv \frac{\beta(C_f - C_s)}{\alpha[\rho_s L_s + \rho_s c_s(T_i - T_s)]/\rho_f c_f} \gg 1, \tag{5}$$

where α is the coefficient of thermal expansion and β is the equivalent coefficient for the variation of density with composition.

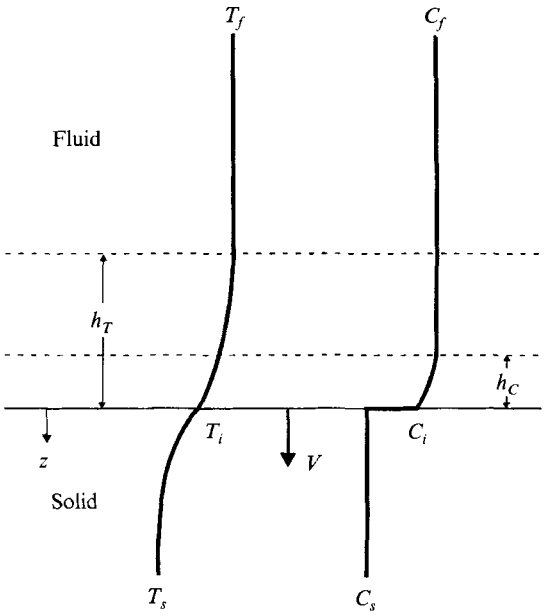

FIGURE 1. The thermal and compositional profiles when a solid dissolves into a fluid at velocity V.

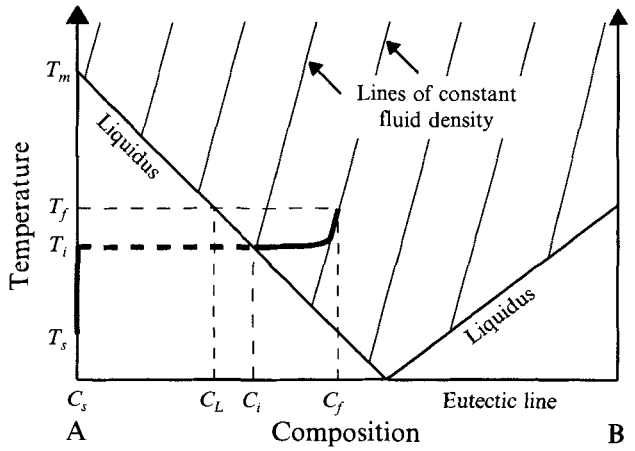

FIGURE 2. The path on a simple phase diagram of the thermal and compositional profiles shown in figure 1. The dotted portion of the path represents the jump in composition at the dissolving interface.

Accordingly, it is envisaged that both the compositional and thermal boundary layers grow diffusively with time t:

$$h_C \sim (Dt)^{1/2}, \quad h_T \sim (\kappa_f t)^{1/2}, \tag{6a, b}$$

where c_f and $\kappa_f \equiv k_f/\rho_f c_f$ are the specific heat and thermal diffusivity of the fluid, until a time τ when the buoyant compositional boundary layer undergoes a Rayleigh–Bénard type of instability that drives vigorous compositional convection. Following Lick (1965) and Howard (1966), instability can be expected when the Rayleigh number Ra of this boundary layer reaches a critical value Ra_c:

$$Ra_c = \frac{g(\rho_f - \rho_i)\, h_C^3}{D\mu}, \tag{7}$$

where g is the acceleration due to gravity and μ is the fluid viscosity. I therefore obtain the estimates

$$h_C = \left(\frac{Ra_c D\mu}{g(\rho_f - \rho_i)}\right)^{1/3}, \quad h_T = h_C\left(\frac{\kappa_f}{D}\right)^{1/2} = \left(\frac{Ra_c^2 \mu^2 \kappa_f^3}{Dg^2(\rho_f - \rho_i)^2}\right)^{1/6}, \quad \tau \approx \left(\frac{Ra_c^2 \mu^2}{Dg^2(\rho_f - \rho_i)^2}\right)^{1/3}. \tag{8a–c}$$

Substitution of (8a) and (3a) into (4a) then yields the prediction that the dissolving velocity is

$$V = \left(\frac{g(\rho_f - \rho_i)\, D^2}{Ra_c \mu}\right)^{1/3}\left(\frac{C_f - C_i}{C_i - C_s}\right), \tag{9}$$

while combining (9), (8b), (3b), (4b) and (1) shows that

$$T_f - T_L(C_i) = \frac{\rho_s L_s + \rho_s c_s (T_L(C_i) - T_s)}{\rho_f c_f}\left(\frac{D}{\kappa_f}\right)^{1/2}\left(\frac{C_f - C_i}{C_i - C_s}\right). \tag{10}$$

From the above analysis, it is concluded that the dissolving rate is given by (9), once C_i is evaluated from (10). I also note that $Ra_c^{-1/3}$ is equivalent to the constant γ in the semi-empirical expression $Nu = \gamma Ra^{1/3}$ that relates the Nusselt number to the Rayleigh number, and is in general a function of the Prandtl number and the aspect ratio of the convecting region (Turner 1979; Denton & Wood 1979; Davaille & Jaupart 1993).

In the above analysis, it has been implicitly assumed that the distance $(D\tau)^{1/2}$ over which compositional diffusion occurs is large in comparison with the distance $V\tau$ that the solid has dissolved in the time τ for instability. From (8a,), (8c) and (9), it is found that

$$V\tau \approx h_C/\mathscr{C}, \tag{11}$$

where

$$\mathscr{C} \equiv \frac{C_i - C_s}{C_f - C_i}. \tag{12}$$

Equations (9) and (10) are therefore asymptotically correct when $\mathscr{C} \gg 1$, a condition that is closely analogous to the condition that the Stefan number is large during melting driven by vigorous compositional convection (see Kerr 1994). If $\mathscr{C}$ is smaller however (i.e. $\mathscr{C} \gtrsim 1$), then (11) suggests that h_C is more accurately estimated by

$$h_C = \left(\frac{Ra_c D\mu}{g(\rho_f - \rho_i)}\right)^{1/3}\left(1 + \frac{1}{\mathscr{C}}\right), \tag{13}$$

which results in V and $T_f - T_i$ being given by

$$V = \left(\frac{g(\rho_f - \rho_i)\, D^2}{Ra_c \mu}\right)^{1/3}\left(\frac{C_f - C_i}{C_f - C_s}\right), \tag{14}$$

and

$$T_f - T_i(C_i) = \frac{\rho_s L_s + \rho_s c_s (T_L(C_i) - T_s)}{\rho_f c_f}\left(\frac{D}{\kappa_f}\right)^{1/2}\left(\frac{C_f - C_i}{C_f - C_s}\right). \tag{15}$$

The presence of D in (14) reflects the fact that dissolution is primarily dependent on the diffusion of composition. The dependence on the diffusion of heat enters only weakly through (15), and in the limit of $D/\kappa_f \to 0$, then $T_i \to T_f$, $C_i \to C_L \equiv T_L^{-1}(T_f)$ (see figure 2), $\rho_i \to \rho_L \equiv \rho_f(C_L, T_f)$ and the dissolution is entirely due to compositional diffusion:

$$V = \left(\frac{g(\rho_f - \rho_L)\, D^2}{Ra_c \mu}\right)^{1/3}\left(\frac{C_f - C_L}{C_f - C_s}\right). \tag{16}$$

This control by compositional diffusion breaks down, however, when $\mathscr{C} \ll 1$. In this important limit where dissolving undergoes a transition to melting, the compositional profile becomes very nonlinear, equation (3*a*) is no longer accurate, and a new scaling analysis is required (which is presented in the Appendix).

2.2. *Dissolving a roof*

In the case of dissolving a roof, compositional convection will occur if the density of the interfacial fluid is greater than that of the far-field fluid. The dissolving rate will be given by (14) and (15), with $\rho_f - \rho_i$ replaced by $\rho_i - \rho_f$, provided that the unstable compositional buoyancy is much greater than the unstable thermal buoyancy ($\mathscr{R} \gg 1$). In opposite limit, $\mathscr{R} \ll 1$, the heat transfer to the dissolving interface will be driven by thermal convection. The thickness of the thermal boundary layer is then no longer given by (8*b*), but by

$$h_T = \left(\frac{Ra_c \mu \kappa_f}{g\rho_f \alpha (T_f - T_i)}\right)^{1/3}, \tag{17}$$

which leads to the temperature difference (15) being replaced by the smaller value

$$T_f - T_L(C_i) = \frac{\rho_s L_s + \rho_s c_s (T_L(C_i) - T_s)}{\rho_f c_f} \left(\frac{D}{\kappa_f}\right)^{1/2} \left(\frac{C_f - C_i}{C_f - C_s}\right) \mathscr{R}^{1/4}. \tag{18}$$

3. Experiments

In this section two series of experiments are described that were performed to test the scaling analysis presented in §2. In these experiments, either an ice roof or an ice floor was dissolved by contact with an aqueous solution.

3.1. *Roof experiments* (*R*)

In these experiments, a block of bubble-free ice, 20×20 cm^2 in cross-section and 7 cm thick, was inserted into the top of an insulated glass tank to leave a space underneath that was 20×20 cm^2 in cross-section and 53 cm high. An aqueous solution of isopropanol was then added through a hole in the base of the tank until it made contact with the ice. The isopropanol solution was used because its density is less than that of water, and because the anomalous density maximum at 4 °C that is associated with pure water can be eliminated by using a sufficient concentration of isopropanol (Kerr *et al.* 1990).

Five experiments were performed, with far-field concentrations of isopropanol which ranged from 22 to 36.5 wt % (see table 1). For these values, which are illustrated on the phase diagram in figure 3, the unstable compositional buoyancy is much greater than the unstable thermal buoyancy ($\mathscr{R} \gg 1$) and the solution convected vigorously. In all the experiments, the far-field temperature was -6.2 ± 0.5 °C, which corresponds to a liquidus concentration C_L of 16.8 ± 0.8 wt %.

Direct observations of the experiments were supplemented by both photographs and videos. These observations showed that the surface of the dissolving ice was pitted. It was also found that the presence of any air bubbles at the ice interface led to the growth of conical cavities in the ice. This interesting phenomenon has also been observed during the melting of an ice roof and is not well understood (Kerr 1994, §4.3 and figure 8).

Observations of the thickness of the ice block as a function of time demonstrated

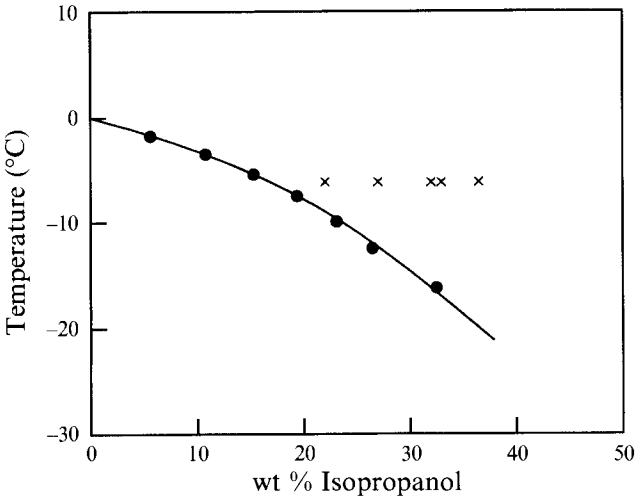

FIGURE 3. Experimental measurements (from Washburn 1926) of the freezing temperature for aqueous solutions of isopropanol. The far-field conditions of the five experiments are indicated by ×.

Quantity	R1	R2	R3	R4	R5	Units	Source
C_f	36.5	33	32	27	22	wt %	
ρ_f	0.954	0.961	0.9635	0.972	0.978	g cm^{-3}	A, C
c_f	4.15	4.29	4.33	4.48	4.57	J g^{-1} cm^{-1}	A
k_f	0.346	0.364	0.369	0.396	0.424	W m^{-1} °C^{-1}	B
ν_f	19.0	17.5	17.1	15.0	12.9	mm^2 s^{-1}	C
C_i	19.7	19.3	19.2	18.5	17.8	wt %	
T_i	−8.1	−7.8	−7.7	−7.3	−6.9	°C	
ρ_i	0.9784	0.9788	0.9789	0.9797	0.9805	g cm^{-3}	
$\mathscr{C}$	1.2	1.4	1.5	2.2	4.3	—	
$\mathscr{R}$	4.4	3.9	3.6	2.8	2.2	—	
$\mathscr{V}$	4.32	3.60	3.35	2.20	1.02	μm s^{-1}	
V_{expt}	1.30	1.23	1.08	0.58	0.37	μm s^{-1}	
$\mathscr{V}/V_{expt}$	0.30	0.34	0.32	0.26	0.37		

TABLE 1. Experimental parameters and results for the dissolving of an ice roof. All the experiments used aqueous solutions of isopropanol at $T_f = -6.2$ °C and ice at $T_s = -9$ °C. $\mathscr{V}$, T_i (in °C) and C_i (in wt % isopropanol) were found using (15) and (19) given the approximate liquidus relationship $T_i = -6.2 + 0.65\,(C_i - 16.8)$ (see (3.22) of Kerr *et al.* 1990). The physical properties of the solutions were obtained from: (A) Washburn (1926), (B) Vargaftik (1975) and (C) direct measurement of ρ_f and $\nu_f = \mu_f/\rho_f$ using calibrated viscometers and hydrometers. Other parameters used are $\rho_s L_s = 306$ J cm^{-3} (Washburn 1926), $\rho_s c_s = 1.832$ J cm^{-3} (Weast 1989), $\alpha = 1.35 \times 10^{-4}$ °C^{-1} (Kerr *et al.* 1990) and $D = 0.24 \times 10^{-5}$ cm^2 s^{-1} (Washburn 1926; Gary-Bobo & Weber 1969).

that the block dissolved at a constant velocity (figure 4). The dissolving velocities are listed in table 1, and are accurate to about 10%. Also given in the table are values of T_i and C_i determined from (1) and (15), and values of the velocity scale $\mathscr{V}$ defined by

$$\mathscr{V} = \left(\frac{g(\rho_f - \rho_i)\,D^2}{\mu}\right)^{1/3} \left(\frac{C_f - C_i}{C_f - C_s}\right). \tag{19}$$

The error in determining $\mathscr{V}$ is about 20%, and is principally due to uncertainties in D and to small variations in T_f during an experiment that lead to small variations in C_i.

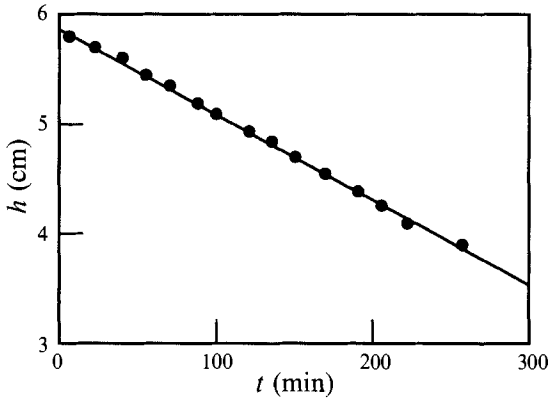

FIGURE 4. The thickness h of the ice block as a function of time during experiment R1. The results show that the melting velocity is constant throughout the experiment.

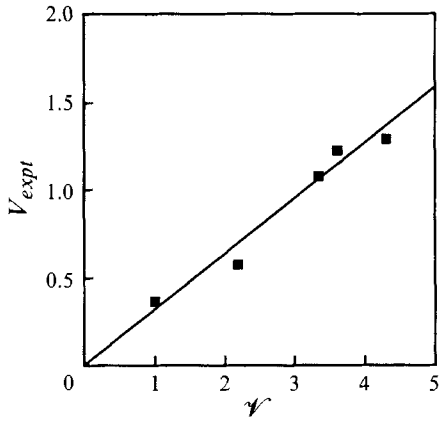

FIGURE 5. The dissolving velocities V_{expt} (in $\mu m\ s^{-1}$) of an ice roof, in comparison with the velocity scale $\mathscr{V}$ defined by (19). The values lie on a straight line with a constant of proportionality of 0.320 ± 0.040.

The dissolving velocities, when plotted against $\mathscr{V}$ in figure 5, are consistent with a straight line whose slope $Ra_c^{-1/3} \approx 0.320 \pm 0.040$.

3.2. *Floor experiments (F)*

These experiments used a $20 \times 20 \times 20\ cm^3$ Perspex tank with a metal base through which cold fluid was pumped. A block of bubble-free ice, about 3 cm thick, was first grown in the base of the tank. An experiment was then started by filling the rest of the tank with an aqueous solution of NaCl. The temperatures and compositions of the solutions are listed in table 2, and are shown on the NaCl–H_2O phase diagram in figure 6. The solution concentrations are accurate to within 0.1 wt %, while the solution temperatures were kept constant to within 0.2 °C by small additions of hot solution during an experiment.

In each of the experiments, vigorous compositional convection was observed. The vigorous convection is due to the buoyancy ratio $\mathscr{R}$ being significantly larger (see table 2) than the critical value of about 2.0 (Kerr 1994, figure 10). It is also noted that small solution concentrations do not lead to small values of $\mathscr{R}$ because these solutions have equally small coefficients of thermal expansion.

Quantity	F1	F2	F3	F4	F5	F6	F7	F8	F9	F10
T_f	−8.8	−12.9	−14.0	−5.9	−2.2	−5.25	−2.3	2.0	4.0	6.0
T_s	−9.4	−14.8	−15.6	−15.6	−8.4	−9.6	−7.6	−11.0	−11.0	−11.0
C_f	22.0	23.2	23.0	22.2	21.68	16.5	15.3	19.3	19.5	20.35
ρ_f	1.176	1.187	1.186	1.176	1.171	1.131	1.120	1.150	1.151	1.157
c_f	3.33	3.30	3.30	3.33	3.35	3.46	3.50	3.40	3.40	3.38
k_f	0.513	0.504	0.502	0.518	0.526	0.527	0.534	0.537	0.540	0.543
ν_f	3.33	4.06	4.23	3.00	2.57	2.57	2.26	2.13	2.02	1.95
α	3.4	3.2	3.1	3.6	3.8	3.0	3.0	3.8	4.0	4.2
C_i	14.6	17.9	18.7	12.2	8.7	10.7	7.8	4.4	2.5	0.58
T_i	−10.5	−14.0	−14.9	−8.4	−5.6	−7.1	−5.0	−2.7	−1.5	−0.35
ρ_i	1.117	1.145	1.152	1.098	1.068	1.085	1.061	1.034	1.018	1.003
$\mathscr{C}$	2.0	3.4	4.4	1.2	0.66	1.9	1.1	0.298	0.147	0.029
$\mathscr{R}$	5.7	6.3	6.4	5.1	4.9	4.9	4.5	4.2	4.0	3.9
$\mathscr{V}$	12.0	6.16	4.60	19.2	31.9	13.5	22.6	49.7	62.2	76.5
V_{expt}	3.15	1.42	1.08	4.30	7.38	3.25	4.70	9.82	13.0	15.7
$\mathscr{V}/V_{expt}$	0.27	0.23	0.24	0.22	0.23	0.24	0.21	0.20	0.21	0.21

TABLE 2. Experimental parameters and results for the dissolving of an ice floor by aqueous solutions of NaCl. $\mathscr{V}$ (in μm s^{-1}), T_i (in °C) and C_i (in wt % NaCl) were found using (15), (19) and the liquidus curve shown in figure 6. The physical properties of the solutions have the same units and sources as indicated in table 1. Also used are values of α (which is shown in units of 10^{-4} $°C^{-1}$), and $D = 10^{-5.144+0.0127T_f}$ cm^2 s^{-1}, where T_f has units of °C, which were both inferred from data in Washburn (1926).

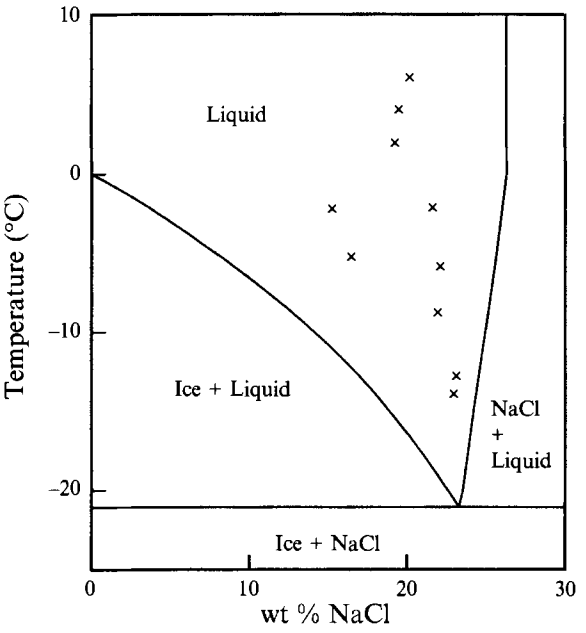

FIGURE 6. The phase diagram for H_2O–NaCl (determined from experimental data given by Washburn 1926 and Weast 1989). The far-field conditions of the ten ice-floor experiments are indicated by ×.

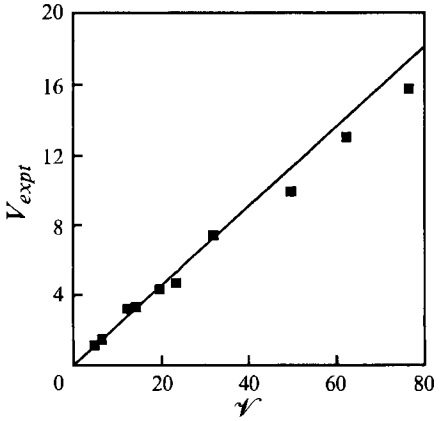

FIGURE 7. The dissolving velocities V_{expt} (in μm s^{-1}) of an ice floor, in comparison with the velocity scale $\mathscr{V}$ defined by (19). The values lie on a straight line with a constant of proportionality of 0.226 ± 0.022.

All the experiments had pitted interfaces, as was also observed by Campbell (1986) and Fang & Hellawell (1988, figure 3). In addition, a small number of larger hemispherical cavities were seen which are taken to be the 'cylindrical cavities' seen by Fang & Hellawell (1988, figures 4 and 5). These cavities were irregularly distributed, infrequent, and probably arose from elongate air bubbles in the ice (Campbell 1986).

The dissolving velocities and the calculated velocity scale $\mathscr{V}$, which are both accurate to about 10%, are plotted against each other in figure 7. The data are seen to lie on a straight line whose slope (0.226 ± 0.022) is lower than the value found in the roof experiments. The difference in these values probably reflects the fact that the roof experiments were somewhat accelerated by the release of a heat of solution (that was

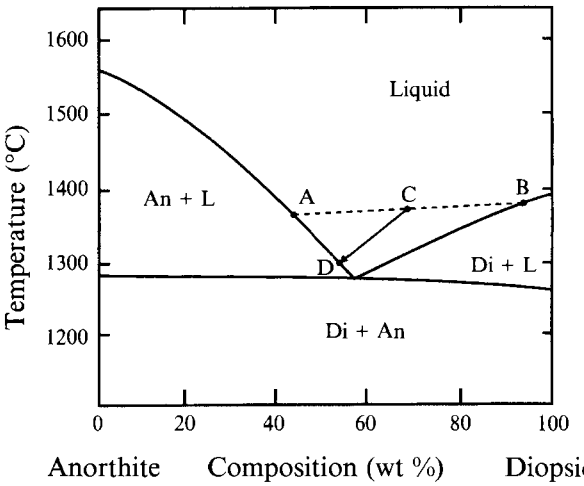

FIGURE 8. The diopside–anorthite phase diagram, which was used by Campbell (1986) to demonstrate that mixing an anorthite-saturated magma (A) with a diopside-saturated magma (B) will result in a magma (C) that is undersaturated with respect to both anorthite and diopside. If this superheated magma is in contact with solid anorthite, the anorthite will be dissolved and the magma will chemically and thermally evolve (as shown by the arrowed path) until it is again on the liquidus (D).

about 25–40 J g^{-1}) while the floor experiments were virtually unaffected by a -3 J g^{-1} heat of solution that is negligible in comparison to the latent heat of the ice. Similar effects of a significant heat of solution have been found in experiments on melting driven by vigorous compositional convection (Kerr 1994, §4.1).

The value of 0.226 found above for $Ra_c^{-1/3}$ can also be compared with values of about 0.16 found for γ in careful measurements of the convective heat flux at high Rayleigh numbers in water (Katsaros *et al.* 1977) and diluted Golden Syrup (Davaille & Jaupart 1993). The higher value obtained in the current experiments may be due to the larger surface area of the pitted dissolving boundary, which should enhance the diffusion of composition to it.

4. Geological application

One important situation where dissolving can be assisted by compositional convection is in large bodies of molten rock in the Earth's crust, which are generally referred to as 'magma chambers'. In some of these chambers, the resident magma cools, crystallizes and chemically evolves until it becomes saturated in the mineral plagioclase. Further cooling of the magma then leads to the growth of a plagioclase-rich layer as the floor of the chamber. This steady evolution is frequently disrupted, however, by the fresh injection into the chamber of a new pulse of the parent magma (Huppert & Sparks 1980). The new magma will typically be hotter, denser, and olivine-saturated, and it is usually input with sufficient momentum that a fountain results (Campbell & Turner 1989). In the fountain, the replenishing and resident magmas are turbulently mixed to produce a magma that is not saturated with respect to either plagioclase or olivine (as is illustrated in figure 8 for the simple and well-known diopside–anorthite chemical system). This superheated magma is therefore able to dissolve the underlying plagioclase floor of the magma chamber.

4.1. *The Bushveld Intrusion*

Campbell (1986) proposed that considerable dissolution occurred immediately after a large replenishment during the formation of the 9 km thick Bushveld Igneous Intrusion in South Africa (Wager & Brown 1968). In this replenishment, which immediately preceded the deposition of the platinum-rich Merensky Reef (Cameron 1982; Campbell, Naldrett & Barnes 1983), it is envisaged that the input magma mixed with a resident magma to form a 1 km thick layer of superheated magma with a density ρ_f of about 2.60 g cm^{-3} (Campbell & Turner 1986, 1989). At the time of this replenishment, the floor of the magma chamber consisted of a thick plagioclase layer (with a composition of about 76 wt % anorthite and about 24 wt % albite) (Wager & Brown 1968; Vermaak 1976; Eales *et al.* 1988). This anorthosite floor has a latent heat $\rho_s L_s$ of about 900 J cm^{-3} (Weill, Hon & Navrotsky 1980; Stebbins, Carmichael & Weill 1983) and a fractionation density ρ_{fr} (i.e. the density of the components selectively added to the melt by dissolution of the crystals (Sparks & Huppert 1984)) of about 2.50 g cm^{-3}. Using also typical estimates (e.g. Huppert & Sparks 1988*b*) of the thermal expansion coefficient ($\alpha = 5 \times 10^{-5}$ °C^{-1}) and heat capacity ($c_f = 1.34$ J g^{-1} °C^{-1}) of the mixed magma, and neglecting the specific heat of the plagioclase in comparison to its latent heat (since its temperature will be only slightly less than that of the overlying magmas), the buoyancy ratio is estimated to be

$$\mathscr{R} = \frac{\rho_f - \rho_{fr}}{\alpha \rho_s L_s / c_f} = 3.0. \tag{20}$$

This calculated ratio of the unstable compositional buoyancy to the stabilizing thermal buoyancy is larger than the critical value of about 2.0 that is necessary to sustain vigorous compositional convection (Kerr 1994).

Since the dissolution of the anorthosite was able to drive vigorous compositional convection, the theoretical and experimental results in this paper can be used to determine the rate at which it occurred. Equation (15) predicts that, for typical values of $D = 10^{-8}$ cm^2 s^{-1} (e.g. Hofmann 1980; Watson 1982; Zhang, Walker & Lesher 1989; Van der Laan & Wyllie 1993) and $\kappa_f = 8 \times 10^{-3}$ cm^2 s^{-1} (e.g. Huppert & Sparks 1988*b*), the temperature difference $T_f - T_i$ (in units of °C) is given by

$$T_f - T_i = 0.3 \left(\frac{C_f - C_i}{C_f - C_s} \right). \tag{21}$$

This temperature difference is very small in comparison with the temperature variations in the phase diagram of the magma (as is indicated by figure 8), so that to a very good approximation $C_i \approx C_L$. Using (14) and estimating the magma viscosity μ as about 300 g cm^{-1} s^{-1}, the predicted dissolving rate (in units of m y^{-1}) is given by

$$V = 3.0 \left(\frac{\rho_f - \rho_L}{Ra_c \rho_f} \right)^{1/3} \left(\frac{C_f - C_L}{C_f - C_s} \right). \tag{22}$$

From the floor dissolving experiments, $Ra_c^{-1/3}$ has a value of about 0.226. Hence for the magma C shown in figure 8, for which $(\rho_f - \rho_L)/\rho_f \approx 0.01$, $C_f = 68.3$ wt %, $C_L = 42.5$ wt % and $C_s = 0$ wt %, the dissolving velocity is initially

$$V = 5.5 \text{ cm y}^{-1}, \tag{23}$$

which corresponds to initial boundary-layer thicknesses of about $h_C = 0.35$ mm and $h_T = 31$ cm.

For comparison, it is noted that the dissolving velocity given by (23) is much greater than the probable solidification rate (~ 0.1 cm y^{-1}) of the Bushveld intrusion (see Kerr & Tait 1986), but is much smaller than the rate (3–20 m y^{-1}) at which a basaltic magma chamber can melt its roof (Huppert & Sparks 1988*a*, *b*; Kerr 1994). The dissolution will cause a layer of magma C of initial thickness $h = 1$ km to cool at a rate

$$\frac{\mathrm{d}T_f}{\mathrm{d}t} = -\frac{V\rho_s L_s}{\rho_f c_f h} \approx 0.013\ ^\circ\mathrm{C\ y^{-1}}, \tag{24}$$

and to decrease in diopside content at a rate

$$\frac{\mathrm{d}C_f}{\mathrm{d}t} = -\frac{V(\rho_f C_f - \rho_s C_s)}{\rho_f h} \approx 0.0037\ \mathrm{wt\ \%\ y^{-1}}. \tag{25}$$

This dissolution of the anorthosite continued until the vigorously convecting magma thermally and compositionally evolved to the point where it began to crystallize and deposit the Merensky Reef chromitite and pyroxenite.

It is important to note that the dissolving calculations above assume that the floor of the magma chamber is completely solid. In reality, however, the floor will be only partially solid, with a porosity that will vary with depth, and which will depend on the magma viscosity, the vigour of the convection, and the rate at which the chamber cools (Sparks *et al.* 1985; Campbell 1987). When the floor is porous, convective exchange can occur between the interstitial magma and the overlying mixed magma (Kerr & Tait 1985). The convection takes the form of 'fingers' of dense magma that penetrate downwards into the porous medium with a velocity

$$V = 0.55\frac{kg(\rho_U - \rho_L)}{\epsilon \mu_L^{0.6}\mu_U^{0.4}}, \tag{26}$$

where k is the permeability, ϵ is the porosity, and L and U refer to lower (interstitial) and upper (mixed) magmas respectively. For finger penetration to significantly accelerate dissolution, their velocity must be greater than the dissolving velocity given by (23), which will require a local floor porosity of at least 0.15 (see figure 7*a* of Kerr & Tait 1985). Both textural and isotopic evidence suggests that porosities were typically small in the Bushveld (Wager & Brown 1968; Campbell 1987), which is consistent with the generally flat contact (with very gentle 'dimples') at the base of the Merensky Reef. Parts of the Reef are however disrupted by large 'potholes' (Campbell 1986; Ballhaus 1988). These potholes appear to be related to fluids released during the metamorphism of sediments underlying the Bushveld: such fluids could lead either to larger porosities in parts of the floor, or to the formation of deep 'fumeroles' in the floor that the replenishing magma is able to penetrate. For fumeroles to be important, flow velocities within them must be greater than the dissolving velocity of the interface, a condition that is satisfied if their diameters are greater than about 40 μm (assuming a magma viscosity μ of 300 g cm^{-1} s^{-1} and a density difference $\rho_U - \rho_L$ of 0.05 g cm^{-3}).

4.2. *The Rhum Intrusion*

The Rhum Intrusion in Northwest Scotland is another location where the magma chamber has undergone many replenishments with dense picritic magma (Wager & Brown 1968). At the contact between cyclic units 11 and 12 of this intrusion, Young (1984) observed several structural features (a dimpled contact, potholes, and an

intervening chrome-spinel layer) which he interpreted as being due to dissolution of the chamber floor after its replenishment. The floor at this time consisted of about 85% plagioclase, 10% augite and 5% olivine (Wager & Brown 1968, pp. 268, 287), which has a fractionation density of about 2.55 g cm^{-3} (Sparks & Huppert 1984) and a latent heat of about 1100 J cm^{-3}. Using the compositions given by Tait (1985) for the replenishing and resident magmas, together with his estimate that the magmas contained about 1 wt% water, the density of the superheated mixed magma can be estimated to be about 2.67 g cm^{-3}, which implies a buoyancy ratio of about 2.9. This value of the buoyancy ratio is large enough for dissolution to be driven by vigorous compositional convection, at rates similar to that estimated by (23) for the Bushveld anorthosite.

In dramatic contrast with the contact between units 11 and 12, the contact between units 10 and 11 does not show similar evidence of dissolution after this previous replenishment of the magma chamber. This observation can be understood by noting that the upper part of unit 10 consists of about 55% plagioclase, 25% augite and 20% olivine (Wager & Brown 1968, pp. 268, 272; Tait 1985, p. 472). This gabbroic assemblage has a much larger fractionation density (about 2.65 g cm^{-3}), which results in a buoyancy ratio ($\mathscr{R} \approx 0.5$) that is far too small to support vigorous compositional convection and significant dissolution. The upper 10 m of the gabbro is however enriched in magnesium, which suggests that the floor was porous enough to allow limited convective exchange between the interstitial and overlying magmas (Tait 1985; Kerr & Tait 1985).

5. Conclusions

In this paper I have examined the dissolution of a solid that has been placed in contact with a solution whose composition is different to that of the solid. During the dissolution, the liquid at the interface will have a temperature and composition that are intermediate between that of the solid and that of the solution. The interfacial fluid will therefore have a different density to that of the solution, and in many situations this will give rise to convective motions (Woods 1992). The current paper investigates the simple case where the dissolving occurs at a horizontal floor or roof, and is driven by vigorous compositional convection. A scaling analysis was used to derive theoretical expressions for both the rate of dissolution and the interfacial concentration.

Experiments were then performed in which an ice roof or floor was dissolved in contact with aqueous solutions. The measured dissolving velocities are consistent with the scaling theory, and also suggest that the rate of dissolving is enhanced by the pitted nature of the interface and by the release of a significant heat of solution.

The results of this study are likely to have a diverse range of applications. One such application to replenished magma chambers has been examined, where dissolution velocities of a few centimetres per year are predicted. In many applications, the geometry of the solid will be more complicated than the simple one-dimensional case considered here (e.g. Kerr 1995). These situations will require further theoretical, experimental and numerical studies, but should be assisted by the physical understanding gained from the current work.

I gratefully acknowledge helpful comments from Ian Campbell, Herbert Huppert, John Lister, Bob Loucks, Steve Tait, Stewart Turner, Andy Woods, and Grae Worster, and the technical assistance of Tony Beasley, Derek Corrigan and Ross Wylde-

Browne. The work benefited from a visit to the Institute of Theoretical Geophysics, Cambridge, with the financial support of The British Council.

Appendix. The transition from dissolving to melting

When $\mathscr{C} \ll 1$, rapid movement of the interface (i.e. $V \gg D/h_C$) will result in a very nonlinear compositional profile, which is approximately given by

$$C(z) \approx C_i + (C_f - C_i)\, \mathrm{e}^{-V(h_C+z)/D}, \quad \text{where} \quad 0 > z > -h_C. \tag{A 1}$$

The resulting compositional flux F_C to the interface is

$$F_C \approx V(C_f - C_i)\, \mathrm{e}^{-Vh_C/D}, \tag{A 2}$$

which when equated to (4a) yields

$$V \approx (D/h_C) \ln (1/\mathscr{C}). \tag{A 3}$$

In this limit of rapid interfacial movement, the boundary layer estimates that were given by (8a–c) are now replaced by

$$h_C \sim \left(\frac{PV\mu_i}{g(\rho_f - \rho_i)}\right)^{1/2}, \quad h_T \sim \left(\frac{P\mu_i \kappa_f^2}{gV(\rho_f - \rho_i)}\right)^{1/4}, \quad \tau \sim \left(\frac{P\mu_i}{gV(\rho_f - \rho_i)}\right)^{1/2} \tag{A 4a–c}$$

(see equations (3), (4) and (6) of Kerr 1994). Substitution of (A 4a) into (A 3) then results in the asymptotic law

$$V \sim \left(\frac{g(\rho_f - \rho_i) D^2}{P\mu_i}\right)^{1/3} \ln^{2/3}\left(\frac{1}{\mathscr{C}}\right), \tag{A 5}$$

which is analogous to equation (A 5) of Kerr (1994). A combination of (A 5), (A 4b), (3b), (4b) and (1) then gives an expression for C_i:

$$T_f - T_L(C_i) \sim \frac{\rho_s L_s + \rho_s c_s (T_L(C_i) - T_s)}{\rho_f c_f} \left(\frac{D}{\kappa_f}\right)^{1/2} \ln^{1/2}\left(\frac{1}{\mathscr{C}}\right). \tag{A 6}$$

If a Stefan number is defined by

$$\mathscr{S}_i = \frac{\rho_s L_s + \rho_s c_s (T_i - T_s)}{\rho_f c_f (T_f - T_i)}, \tag{A 7}$$

(A 5) and (A 6) can be alternatively written as

$$V \sim \left(\frac{g(\rho_f - \rho_i)\kappa_f^2}{P\mu_i \mathscr{S}_i^4}\right)^{1/3} \tag{A 8}$$

and

$$\mathscr{S}_i \sim (\kappa_f/D)^{1/2} \ln^{-1/2}(1/\mathscr{C}). \tag{A 9}$$

Equations (A 5) and (A 8) can then be viewed as providing the link between the dissolving expressions given by (9) and (14), which provide accurate upper and lower bounds on V when $\mathscr{C}$ is large, and the melting expression given by equation (10) of Kerr (1994), which holds when $\mathscr{C} \approx 0$ and $T_i \approx T_m = T_L(C_s)$. Equation (A 9) can also be compared with the dissolving equations (10) and (15), which can be expressed respectively as $\mathscr{S}_i = (\kappa_f/D)^{1/2}\, \mathscr{C}$ and $\mathscr{S}_i = (\kappa_f/D)^{1/2}\, (\mathscr{C} + 1)$.

REFERENCES

BALLHAUS, C. G. 1988 Potholes of the Merensky Reef at Brakspruit Shaft, Rustenburg Platinum Mines: Primary disturbances in the magmatic stratigraphy. *Econ. Geol.* **83**, 1140–1158.

CAMERON, E. N. 1982 The upper critical zone of the Eastern Bushveld Complex – Precursor of the Merensky Reef. *Econ. Geol.* **77**, 1307–1327.

CAMPBELL, I. H. 1986 A fluid dynamic model for potholes of the Merensky Reef. *Econ. Geol.* **81**, 1118–1125.

CAMPBELL, I. H. 1987 Distribution of orthocumulate textures in the Jimberlana Intrusion. *J. Geol.* **95**, 35–54.

CAMPBELL, I. H., NALDRETT, A. J. & BARNES, S. J. 1983 A model for the origin of the platinum-rich sulfide horizons in the Bushveld and Stillwater Complexes. *J. Petrol.* **24**, 133–165.

CAMPBELL, I. H. & TURNER, J. S. 1986 The role of convection in the formation of platinum and chromite deposits in layered intrusions. In *Short Course in Silicate Melts* (ed. C. M. Scarfe), pp. 236–278. Mineral. Assoc. Canada.

CAMPBELL, I. H. & TURNER, J. S. 1989 Fountains in magma chambers. *J. Petrol.* **30**, 885–923.

CARSLAW, H. S. & JAEGER, J. C. 1986 *Conduction of Heat in Solids.* Oxford University Press.

CHIARELI, A. O. P., HUPPERT, H. E. & WORSTER, M. G. 1994 Segregation and flow during the solidification of alloys. *J. Cryst. Growth* **139**, 134–146.

DAVAILLE, A. & JAUPART, C. 1993 Transient high-Rayleigh-number thermal convection with large viscosity variations. *J. Fluid Mech.* **253**, 141–166.

DENTON, R. A. & WOOD, I. R. 1979 Turbulent convection between two horizontal plates. *Intl J. Heat Mass Transfer* **22**, 1339–1346.

EALES, H. V., FIELD, M., DE KLECK, W. J. & SCOON, R. N. 1988 Regional trends of chemical variation and thermal erosion in the Upper Critical Zone, Western Bushveld Complex. *Mineral. Mag.* **52**, 63–79.

FANG, D. & HELLAWELL, A. 1988 The surface morphology of crystals melting under solutions of different densities. *J. Cryst. Growth* **92**, 364–370.

GARY-BOBO, C. M. & WEBER, H. W. 1969 Diffusion of alcohols and amides in water from 4 to 37 °C. *J. Phys. Chem.* **73**, 1155–1156.

HOFMANN, A. W. 1980 Diffusion in natural silicate melts: a critical review. In *Physics of Magmatic Processes* (ed. R. B. Hargraves), pp. 385–418. Princeton University Press.

HOWARD, L. N. 1966 Convection at high Reynolds number. In *Proc. 11th Intl Congr. Appl. Mech., Munich,* pp. 1109–1115. Springer.

HUPPERT, H. E. 1989 Phase changes following the initiation of a hot turbulent flow over a cold solid surface. *J. Fluid Mech.* **198**, 293–320.

HUPPERT, H. E. & SPARKS, R. S. J. 1980 The fluid dynamics of a basaltic magma chamber replenished by influx of hot, dense ultrabasic magma. *Contrib. Mineral. Petrol.* **75**, 279–289.

HUPPERT, H. E. & SPARKS, R. S. J. 1988*a* Melting the roof of a chamber containing a hot, turbulently convecting fluid. *J. Fluid Mech.* **188**, 107–131.

HUPPERT, H. E. & SPARKS, R. S. J. 1988*b* The generation of granitic magmas by intrusion of basalt into continental crust. *J. Petrol.* **29**, 599–624.

KATSAROS, K. B., LIU, W. T., BUSINGER, J. A. & TILLMAN, J. E. 1977 Heat transport and thermal structure in the interfacial boundary layer measured in an open tank of water in turbulent free convection. *J. Fluid Mech.* **83**, 311–335.

KERR, R. C. 1994 Melting driven by vigorous compositional convection. *J. Fluid Mech.* **280**, 255–285.

KERR, R. C. 1995 Convective crystal dissolution. *Contrib. Mineral. Petrol.* (submitted).

KERR, R. C. & TAIT, S. R. 1985 Convective exchange between pore fluid and an overlying reservoir of denser fluid: a post-cumulus process in layered intrusions. *Earth Planet. Sci. Lett.* **75**, 147–156.

KERR, R. C. & TAIT, S. R. 1986 Crystallization and compositional convection in a porous medium with application to layered igneous intrusions. *J. Geophys. Res.* **91**, 3591–3608.

KERR, R. C., WOODS, A. W., WORSTER, M. G. & HUPPERT, H. E. 1990 Solidification of an alloy cooled from above. Part 1. Equilibrium growth. *J. Fluid Mech.* **216**, 323–342.

LICK, W. 1965 The instability of a fluid layer with time-dependent heating. *J. Fluid Mech.* **21**, 565–576.

SPARKS, R. S. J. & HUPPERT, H. E. 1984 Density changes during the fractionational crystallization of basaltic magmas: fluid dynamic implications. *Contrib. Mineral. Petrol.* **85**, 300–309.

SPARKS, R. S. J., HUPPERT, H. E., KERR, R. C., MCKENZIE, D. P. & TAIT, S. R. 1985 Postcumulus processes in layered intrusions. *Geol. Mag.* **122**, 555–568.

STEBBINS, J. F. CARMICHAEL, I. S. E. & WEILL, O. E. 1983 The high temperature liquid and glass heat contents and the heats of fusion of diopside, albite, sanadine and nepheline. *Am. Mineralogist* **68**, 717–730.

TAIT, S. R. 1985 Fluid dynamic and geochemical evolution of cyclic unit 10, Rhum, Eastern Layered Series. *Geol. Mag.* **122**, 469–484.

TURNER, J. S. 1979 *Buoyancy Effects in Fluids*. Cambridge University Press.

VAN DER LAAN, S. R. & WYLLIE, P. J. 1993 Experimental interaction of granitic and basaltic magmas and implications for mafic enclaves. *J. Petrol.* **34**, 491–517.

VARGAFTIK, N. B. 1975 *Tables on the Thermodynamic Properties of Liquids and Gases*. John Wiley & Sons.

VERMAAK, C. F. 1976 The Merensky Reef – Thought on its environment and genesis. *Econ. Geol.* **71**, 1270–1298.

WAGER, L. R. & BROWN, G. M. 1968 *Layered Igneous Rocks*. Edinburgh: Oliver & Boyd.

WASHBURN, E. W. (Ed.) 1926 *International Critical Tables of Numerical data: Physics, Chemistry and Technology*. National Academic Press.

WATSON, E. B. 1982 Basalt contamination by continental crust: some experiments and models. *Contrib. Mineral. Petrol.* **80**, 73–87.

WEAST, R. C. (Ed.) 1989 *CRC Handbook of Chemistry and Physics*. CRC Press.

WEILL, D. F., HON, R. & NAVROTSKY, A. 1980 The igneous system $CaMgSi_2O6$–$CaAl_2Si_2O_8$–$NaAlSi_3O_8$: variations on a classical theme by Bowen. In *Physics of Magmatic Processes* (ed. R. B. Hargraves), pp. 49–92.

WOODS, A. W. 1992 Melting and dissolving. *J. Fluid Mech.* **239**, 429–448.

YOUNG, I. M. 1984 Mixing of supernatant and interstitial fluids in the Rhum Layered Intrusion. *Mineral. Mag.* **48**, 345–350.

ZHANG, Y., WALKER, D. & LESHER, C. E. 1989 Diffusive crystal dissolution. *Contrib. Mineral. Petrol.* **102**, 492–513.